Progress In Electromagnetics Research C, Vol. 53, 99–109, 2014

A Compact and Multiband Fractal-Inspired Planar Dipole Antenna Loaded with Series Capacitances and a Parasitic Element

Saeid Jamilan*, Farzad Tofigh, and Mohammad N. Azarmanesh

Abstract—A novel compact and multiband dipole antenna with a planar fractal-inspired configuration is presented. Several series capacitances and a parasitic element are employed as loading. Results show that the loading improves the impedance matching and enables the proposed antenna to radiate at multiple frequency bands which are not harmonically related. In addition, the proposed loaded dipole antenna offers a high degree of miniaturization in comparing with the unloaded host dipole antenna. The simulated $|S_{11}|$ response of the proposed loaded dipole antenna shows five distinct resonant bands with the center resonant frequencies of 1.52 GHz, 3.62 GHz, 4.6 GHz, 6.9 GHz, and 9.43 GHz with the associated -10 dB bandwidths of 50 MHz, 470 MHz, 170 MHz, 1.15 GHz, and 360 MHz, respectively. A fabricated prototype has compact dimensions of the 37 mm $\times$ 14 mm $\times$ 1.6 mm, and exhibits good agreement between the measured and simulated S-parameters.

1. INTRODUCTION

Nowadays, most modern communication applications require that the antennas have compact size, easy fabrication process, planar structure, and multiband performance. Different conventional approaches are used to design multiband antennas such as modifying a conventional microstrip patch antenna either by operating at different harmonics, using multi-branched strips, adding an additional resonator, or by reactively loading the patch antenna with shorting pins [1–7]. However, the traditional approaches have some disadvantages like increasing the physical dimensions of the antenna. On the other hand, designing compact antennas is imperative in practical applications. In theory, the total effective length of dipole arms is usually as half as that of the operating wavelength. Accordingly, designing small antennas can find various important applications. Several promising compact printed dipole antennas with multiband or wideband operations have been reported in the literature [8–13]. A wideband dipole antenna using parasitic patches has been presented in [14]. By means of employing a parasitic element near the radiating arms, two planar dipole antennas could produce tree resonant frequency bands [15, 16]. In addition, a compact planar dipole antenna loaded with series lumped capacitances and shunt lumped inductances based on the metamaterial transmission line theory, has been proposed in [17] while this approach was effective to reduce the electrical size of the antenna.

A general model for a conventional transmission line (TL) unit cell consists of a series inductance L and a shunt capacitance C while the series inductance is provided by the current flow on the TL unit cell and shunt capacitance is formed based on the electric field between the TL and the ground plane [18]. In the TL unit cell designing, the gaps which are etched on the TL, provide series capacitances. The input impedance of an antenna can be manipulated by loading it with reactive series capacitances and this approach can result in multiband impedance matching.

Furthermore, implementing the fractal-inspired structure can causes the dipole antenna to have a multiband operation and also provides a suitable medium for the placement of the series capacitances.

Received 11 July 2014, Accepted 2 September 2014, Scheduled 8 September 2014
* Corresponding author: Saeid Jamilan (saeid.jamilan@gmail.com).
The authors are with the Department of Electrical Engineering, Urmia University, Urmia, Iran.

It has been verified that applying fractal geometries can provide multiband and miniaturization features [19–23]. In this article, we have used the advantages of employing series capacitive loadings, parasitic elements, and fractal-inspired configurations, besides each other, in order to introduce a novel dipole antenna. A tree-shaped fractal structure is utilized as two host dipole arms. The series capacitances are formed by the etched gaps on the dipole arms. Besides, the parasitic element works as a coupled resonator on the backside of the substrate. This configuration causes the antenna to radiate at several distinct frequency bands. In addition, the proposed dipole antenna offers a large degree of miniaturization at first resonant frequency band in comparing with the unloaded host dipole antenna. Its compact size, planar configuration, simple fabrication, multiband operation, and high-efficiency radiation make it a good candidate for portable devices.

This paper is organized as follows. In Section 2.1, the design of the proposed host dipole antenna is presented. In Sections 2.2 and 2.3, the designing procedures of series capacitive loadings and parasitic element and how these designed loadings separately influence the proposed antenna's performance, have been illustrated. In Section 2.4, the design of proposed dipole antenna loaded with both series capacitances and parasitic element is described. In Section 3, a prototype of the proposed loaded dipole antenna is fabricated and measured, and the simulated and measured results are presented. The conclusion is given in Section 4.

2. ANTENNA DESIGN

2.1. Unloaded Host Dipole Antenna Design

Configuration of the host dipole antenna with its geometrical parameters is shown in Figure 1. The proposed antenna is designed on a FR-4 substrate with thickness of 1.6 mm, dielectric constant of 4.4, and loss tangent of 0.025. The thickness of used copper layers is 30 μm. A 50-Ω SMA connector directly feeds the dipole arms by an edge-coupled coplanar strip (CPS) line. This type of feeding is used in [24] to feed a bow-tie planar dipole antenna. As shown in Figure 1(b), center conductor of SMA connector is connected to the left CPS conductor and the outer surface of SMA connector is connected to the right CPS conductor. The CPS line is a balanced line which connects the unbalanced SMA connector to the dipole arms. In fact, the CPS line works as a TL transformer. However, some low-magnitude currents flowing on the outer surface of the SMA connector, can be caused by the inherent imbalance between the balanced CPS line and the unbalanced SMA connector. These currents on the outside of the SMA connector surface, can cause the connector to slightly radiate. This may cause a distortion in the radiation pattern of the dipole antenna. The simulated reflection coefficient of the proposed host dipole antenna is plotted in Figure 2. All of the simulations and optimizations are performed using CST Microwave Studio. It can be seen that the multiband resonant behavior is achieved by designing the host dipole antenna based on a fractal-inspired geometry. As shown in Figure 2, the proposed host dipole antenna has two resonances matched below −10 dB at 2.42 GHz, and 6 GHz with −10 dB bandwidths of 218 MHz, and 1.56 GHz, respectively.

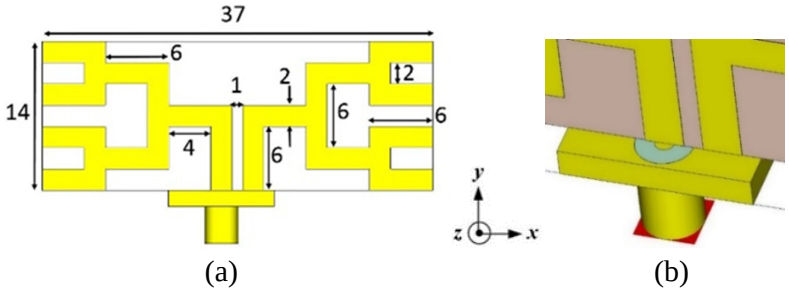

Figure 1. Geometry of the proposed host dipole antenna (mm). (a) Top view. (b) Configuration of the feeding part.

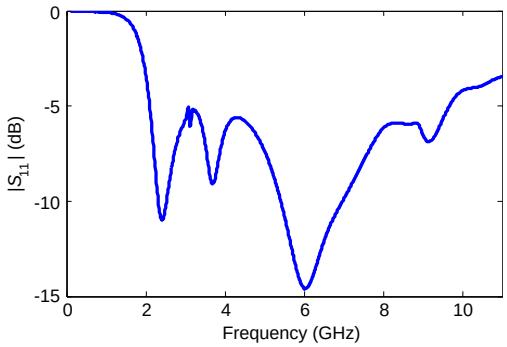

Figure 2. Simulated $|S_{11}|$ response of the proposed host dipole antenna of Figure 1.

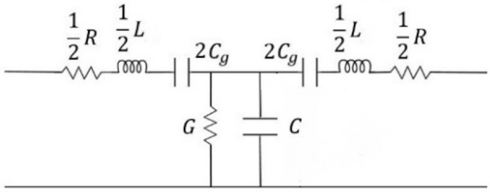

Figure 3. Equivalent circuit of a conventional TL unit cell loaded with a series capacitance C_g.

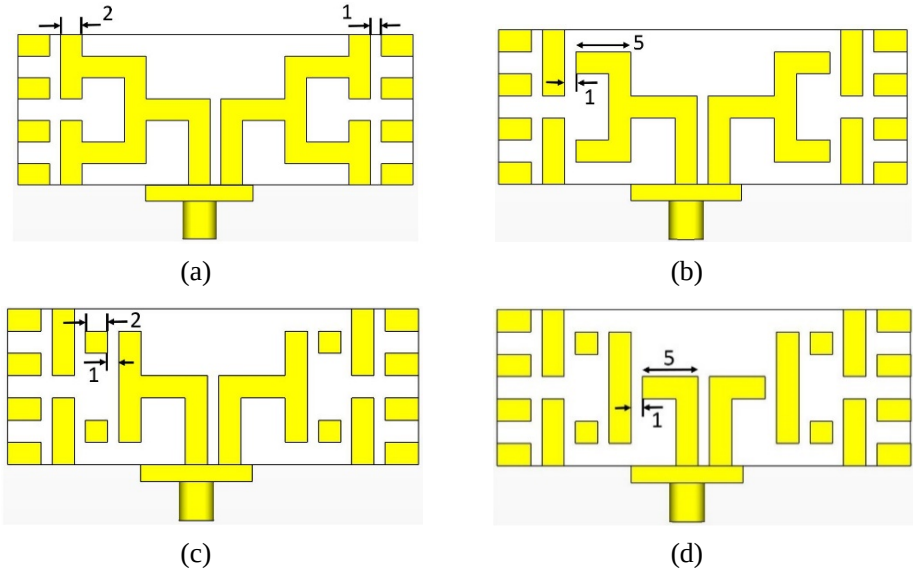

Figure 4. Top view of the proposed host dipole antenna loaded with series capacitive loadings for four steps of the designing procedure (mm). (a) First step. (b) Second step. (c) Third step. (d) Fourth step.

2.2. Capacitive Loadings Design

An effective equivalent circuit for a conventional TL unit cell loaded with a series capacitance C_g is depicted in Figure 3 where R and G are the series resistance and shunt conductance of a lossy TL unit cell, respectively. As explained, the series capacitances can be formed using gaps which are etched on the dipole arms. In order to investigate the effect of series capacitive loading on the performance of proposed host dipole antenna, the series capacitive gaps have been etched gradually on the dipole arms in four steps. Each of the etched capacitive gaps has 1 mm width. Employing Agilent-ADS Software, the series gap capacitances are estimated to be $C_g = 0.02$ pF. Designing procedure of the capacitive loadings is shown in Figure 4. As shown in Figure 4(a), in the first step, the capacitive gaps have been etched on the end branches of tree-shaped dipole arms. Then, as shown in Figures 4(b), (c), and (d), the dipole arms have been loaded with more capacitive gaps step-by-step. The simulated $|S_{11}|$ responses of the host dipole antenna loaded with series capacitances for four stages of capacitive loadings designing, are plotted in Figure 5. It can be seen that adding more capacitive gaps in the second and third steps, makes the two simulated resonances deeper by improving the impedance matching, while, based on the simulated reflection coefficient of the loaded dipole antenna of fourth step, etching the capacitive gaps on the beginning part of the dipole arms causes the antenna to has only a weak resonance at nearly

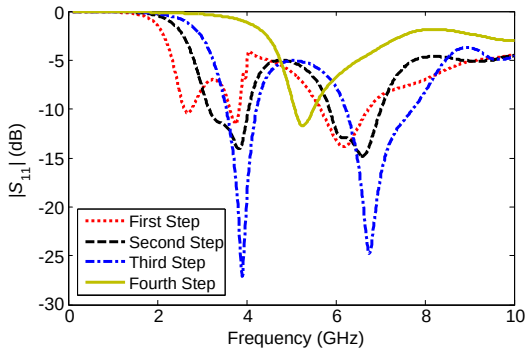

Figure 5. Simulated $|S_{11}|$ responses of the proposed loaded dipole antennas of Figure 4 for four steps of capacitive loadings designing.

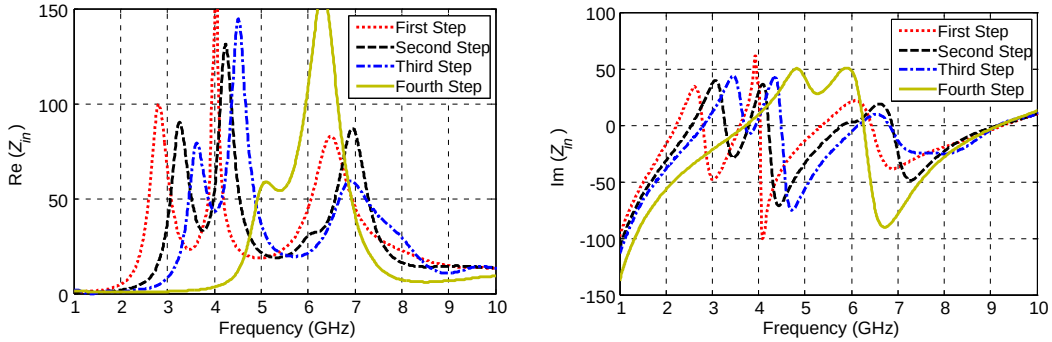

Figure 6. Simulated input impedances of the proposed loaded dipole antennas of Figure 4 for four steps of capacitive loadings designing. (a) Real part. (b) Imaginary part.

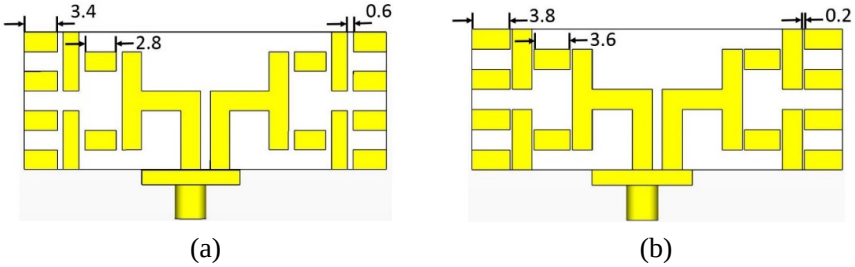

Figure 7. Geometry of the proposed loaded dipole antenna of Figure 4(c) for two different widths of capacitive gaps (mm). (a) 0.6 mm. (b) 0.2 mm.

5.2 GHz. Therefore, we can infer that the proposed loaded dipole antenna of Figure 4(c) shows better impedance matching compared to the loaded dipole antennas of Figures 4(a), (b), and (d).

The simulated results in Figure 6 show the real (resistance) and imaginary (reactance) parts of the input impedances of the proposed antennas of Figure 4 for four steps of capacitive loadings designing. In order to have a very good impedance matching at a resonance with respect to a 50-Ω source, the real and imaginary parts of the input impedance have to be 50-Ω and 0-Ω, respectively, for a same frequency. Therefore, a very low return loss can be achieved when the real and imaginary parts of the input impedance satisfy the mentioned condition for the same frequency. It can be observed from Figure 6 that for the third step of capacitive loadings designing, the real and imaginary parts of the input impedance get closer to 50-Ω and 0-Ω, respectively, for the same frequencies at nearly 3.9 GHz and 6.7 GHz, resulting in a very low return loss. As depicted in Figure 7, the capacitive gaps width of

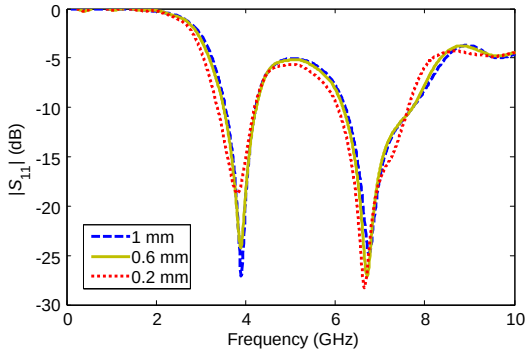

Figure 8. Simulated $|S_{11}|$ responses of the proposed loaded dipole antenna of Figure 4(c) for different widths of capacitive gaps.

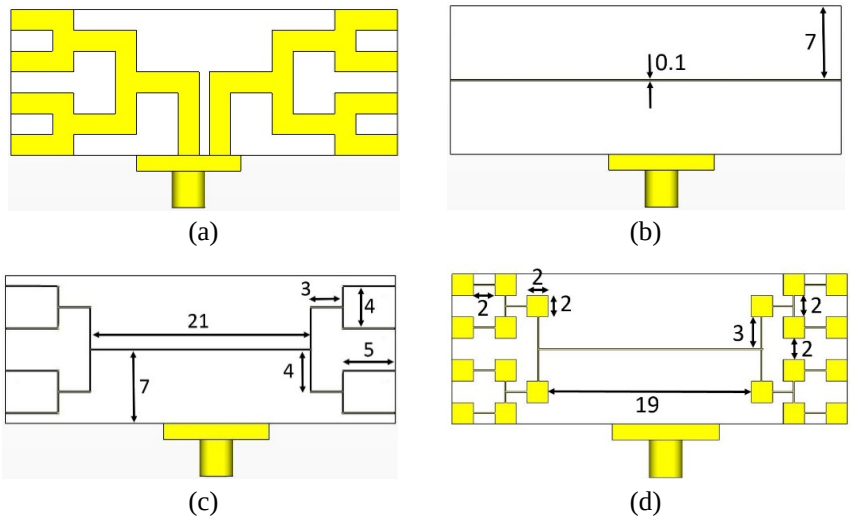

Figure 9. Geometry of the proposed host dipole antenna loaded with three different designs of the parasitic element (mm). (a) Top view. (b) Bottom view of the first design. (c) Bottom view of the second design. (d) Bottom view of the third design.

the designed antenna of Figure 4(c) is decreased from 1 mm to 0.6 mm and 0.2 mm in order to reveal its influence on the proposed antenna's performance. The simulated reflection coefficients of antenna of Figure 4(c) for different widths of the capacitive gaps are plotted in Figure 8. It can be observed that by decreasing the width of etched gaps from 1 mm to 0.2 mm, the first and second resonance frequencies slightly decrease.

2.3. Parasitic Element Design

Due to improve the proposed host antenna's performance, the effect of a parasitic element on the backside of the substrate is investigated in this section. In the first step of parasitic element designing, as shown in Figure 9(b), a straight thin strip is placed on the backside of the substrate as the parasitic element. In next step, as shown in Figure 9(c), the proposed host dipole antenna is loaded with a parasitic element on the backside of the substrate which has a fractal-inspired geometry. This geometry coincides with the tree-shaped fractal geometry of the dipole arms. The aim of this design is to increase the desired influence of coupling between the dipole arms and the parasitic element on the resonant behavior of proposed antenna. In the last step, twenty small rectangular patches have been added to the previous designed parasitic element. Thin inductive strips join these small rectangular patches beneath one of the dipole arms, to other rectangular patches beneath the other dipole arm. The geometry of the

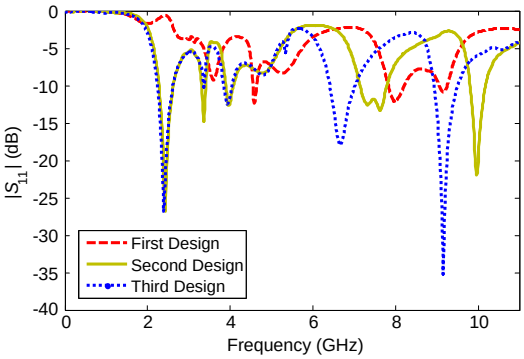

Figure 10. Simulated $|S_{11}|$ responses of the proposed dipole antennas of Figure 9 loaded with three different designs of the parasitic element.

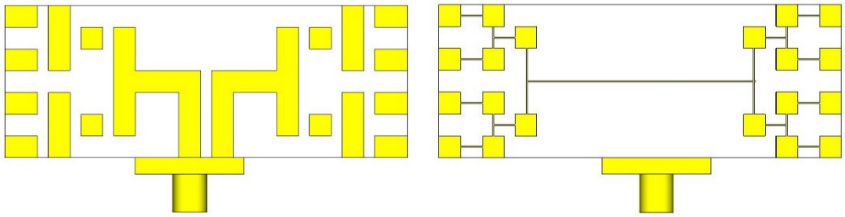

Figure 11. Geometry of the proposed dipole antenna loaded with both series capacitances and parasitic element. (a) Top view of the loaded dipole antenna. (b) Bottom view of the loaded dipole antenna.

designed parasitic element with small patches is indicated in Figure 9(d). The simulated $|S_{11}|$ responses of the proposed host dipole antenna loaded with different versions of the parasitic element shown in Figure 9, are plotted in Figure 10. It can be seen that when the host dipole antenna is loaded with a fractal-inspired parasitic element, it is able to offer more resonances with better impedance matching compared to the host antenna loaded with a simple thin straight strip as the parasitic element. In addition, it can be observed that adding the small patches to the tree-shaped parasitic element, decreases the last two resonant bands frequencies and makes them deeper. Therefore, it can be concluded that small patches has a positive effect on the proposed antenna's performance.

2.4. Dipole Antenna Loaded with Both Series Capacitances and Parasitic Element

Based on the obtained results of above sections, it can be inferred that when the proposed host dipole antenna is only loaded with series capacitances shown in Figure 4(c), it shows two deep resonances. On the other hand, when the proposed host dipole antenna is only loaded with the tree-shaped parasitic element, it offers five resonances. It can be predicted that by loading the proposed host dipole antenna with both series capacitances and parasitic element, it can offer a multiband performance while all resonances are well-matched below -10 dB. The geometry of the proposed host dipole antenna loaded with both series capacitances and parasitic element is shown in Figure 11. Regarding the obtained results of above sections, the capacitive loadings and parasitic element designs of Figures 4(c) and 9(d), respectively, are chosen to design the loaded dipole antenna of Figure 11. The simulated reflection coefficients of the proposed unloaded host dipole antenna of Figure 1 and loaded dipole antenna of Figure 11 are plotted in Figure 12. It can be seen that the multiband behavior is achieved by loading the host fractal-inspired dipole antenna with series capacitive gaps and a parasitic element in order to form a loaded dipole antenna. The proposed loaded dipole antenna has more resonant frequency bands compared to the host dipole antenna. Based on the simulated $|S_{11}|$ response of the proposed loaded dipole antenna of Figure 11, the resonances are centered at 1.52 GHz, 3.62 GHz, 4.6 GHz, 6.9 GHz,

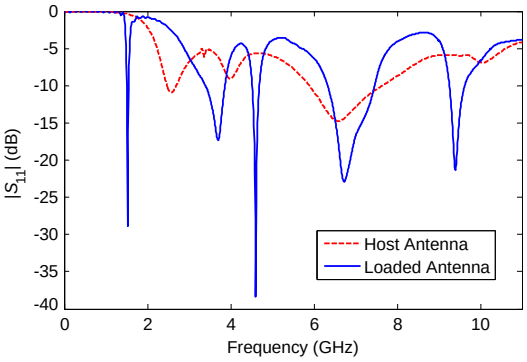

Figure 12. Simulated $|S_{11}|$ responses of the proposed host dipole antenna of Figure 1 and loaded dipole antenna of Figure 11.

and 9.43 GHz and have −10 dB bandwidths of 50 MHz, 470 MHz, 170 MHz, 1.15 GHz, and 360 MHz, respectively. It can be observed that all simulated resonances of proposed loaded dipole antenna of Figure 11, are well-matched below −10 dB. We can infer that the employed loading improves the impedance matching of the proposed dipole antenna with respect to the 50-Ω source. By comparing the obtained results of Figure 10 (for the third design of the parasitic element) and 12, it can be concluded that adding the series capacitive loadings, while the antenna has been also loaded with the parasitic element before, decreases the first resonance frequency from 2.4 GHz to 1.52 GHz and makes the second and third resonances deeper.

The lowest resonant frequency of the proposed loaded dipole antenna of Figure 11 at 1.52 GHz, offers a large degree of miniaturization compared to the host dipole antenna of Figure 1. The loaded dipole antenna exhibits 0.9 GHz reduction of the lowest resonant frequency, compared to the host dipole antenna which has the lowest resonant frequency of 2.42 GHz. The full size of the proposed loaded dipole antenna is 37 mm × 14 mm × 1.6 mm, or 0.18λ mm × 0.07λ mm × 0.008λ with respect to the free space wavelength λ at the lowest center resonant frequency of 1.52 GHz. Therefore, proposed antenna has an electrically small dimensions in comparing with a conventional dipole antenna with 0.5λ length.

3. EXPERIMENTAL RESULTS AND DISCUSSIONS

Figure 13 shows the fabricated prototype of the proposed loaded dipole antenna of Figure 11. The $|S_{11}|$ response of the fabricated antenna is extracted by a vector network analyzer Agilent E8363C and shown in Figure 14. It can be seen that the experimental result and simulated result are in a good agreement

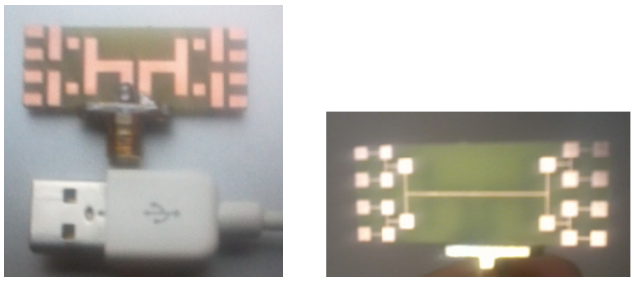

Figure 13. Photographs of the fabricated prototype of proposed loaded dipole antenna of Figure 11. (a) Top view. (b) Bottom view.

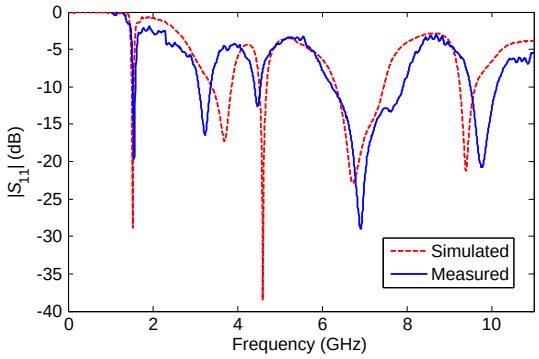

Figure 14. Measured and simulated $|S_{11}|$ responses of the proposed loaded dipole antenna.

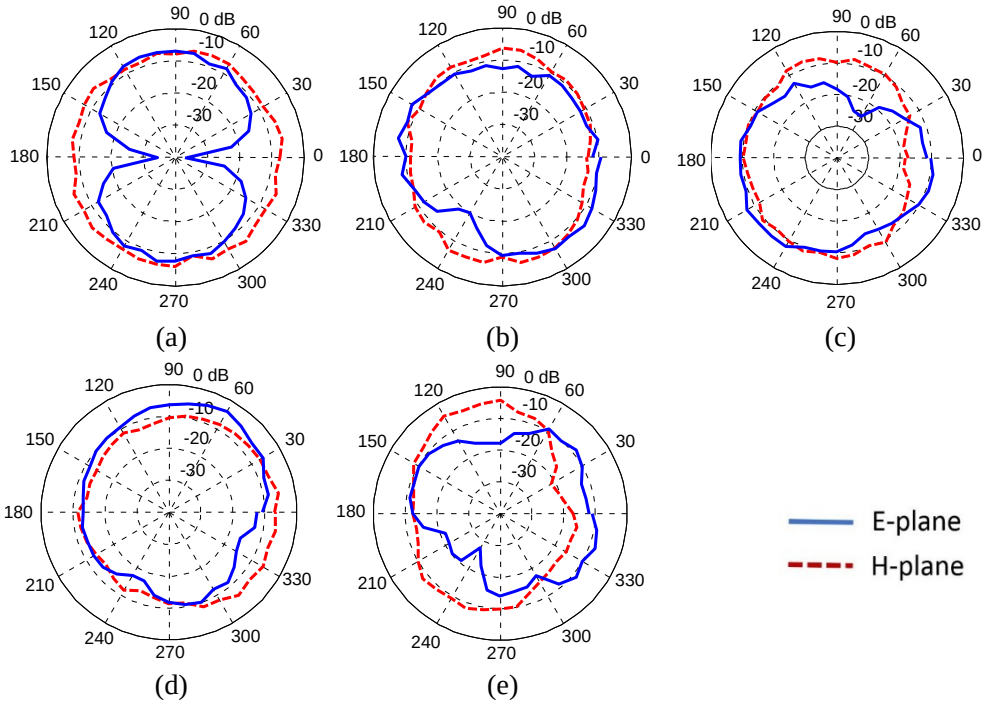

Figure 15. Measured radiation patterns of the fabricated loaded dipole antenna of Figure 13 at (a) 1.55, (b) 3.23, (c) 4.47, (d) 6.91, and (e) 9.76 GHz.

with each other. Some disagreements can be related to either the inaccuracies in the dimensions of the fabricated antenna's elements produced during the fabrication process or measurement equipment or connector or some interferences in measurement environment. The measured radiation patterns of the fabricated loaded dipole antenna of Figure 13 at its measured center resonant frequencies are plotted in Figure 15, where H-plane (yz-plane) and E-plane (xy-plane) radiation patterns at 1.55 GHz, 3.23 GHz, 4.47 GHz, 6.91 GHz, and 9.76 GHz are shown. At the first resonant band, the proposed antenna exhibits an excellent dipolar radiation pattern with a linear x-directed electric field polarization. However in the first resonant band, the proposed loaded dipole antenna has an x-directed linear E-field radiation with high-purity, but in the upper resonant bands, the y-directed currents along the vertical strips of dipole arms, have contribution to the cross-polarization.

Simulated peak gains of the proposed loaded dipole antenna of Figure 11, at center resonant frequencies of 1.52 GHz, 3.62 GHz, 4.6 GHz, 6.9 GHz, and 9.43 GHz are 1.21 dBi, 2.24 dBi, 1.73 dBi, 3.92 dBi, and 3.39 dBi, respectively, and simulated radiation efficiencies at the same resonant frequencies are 86%, 90%, 72%, 78%, and 52%, respectively, while the measured peak gains of the fabricated loaded dipole antenna of Figure 13, at measured center resonant frequencies of 1.55 GHz, 3.23 GHz, 4.47 GHz, 6.91 GHz, and 9.76 GHz are 1.1 dBi, 2.3 dBi, 1.9 dBi, 4.1 dBi, and 3.7 dBi, respectively, and measured radiation efficiencies at same resonant frequencies are 83%, 90%, 70%, 74%, and 55%, respectively. The simulated current distribution on the backside of the substrate at the center resonant frequency of 1.52 GHz is shown in Figure 16. As seen, there is a strong current flow on the thin strips. We can infer that the parasitic element strongly acts as coupled resonator.

In order to investigate the effect of small rectangular patches of parasitic element on the performance of the proposed loaded dipole antenna of Figure 11, the small patches from the parasitic element on the backside of substrate are removed and the simulated $|S_{11}|$ response is shown in Figure 17. It can be seen that when the rectangular patches are removed, the $|S_{11}|$ response of the proposed loaded dipole antenna of Figure 11 changes in all frequency bands except second resonance band. The disadvantage of removing patches is that the proposed antenna shows lower degree of miniaturization with respect to the lowest resonance frequency. On the opposite side, the advantage is that another resonant frequency is added at nearly 7.8 GHz. As shown in Figure 18, a sample of the proposed loaded dipole antenna

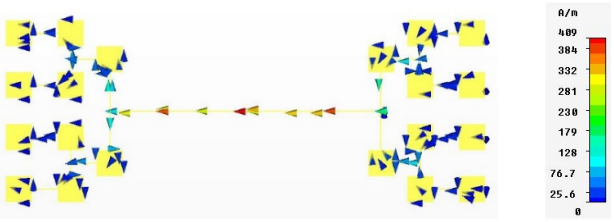

Figure 16. Simulated current distribution on the parasitic element at 1.52 GHz.

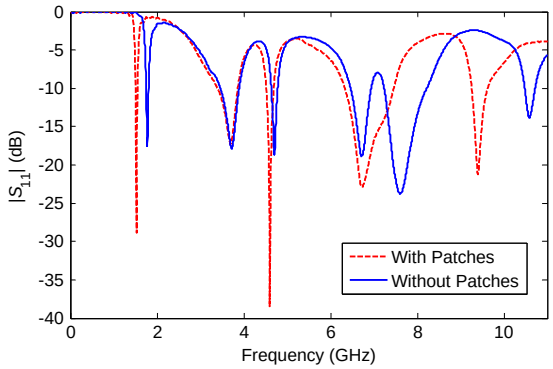

Figure 17. Simulated $|S_{11}|$ responses of the proposed loaded dipole antenna of Figure 11 with and without small patches in the parasitic element structure.

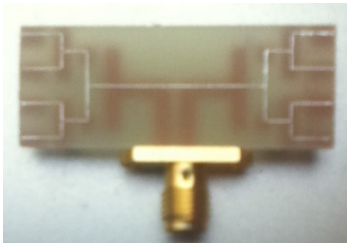

Figure 18. Bottom view photograph of the fabricated prototype of proposed loaded dipole antenna of Figure 11 while the small patches are removed from the parasitic element.

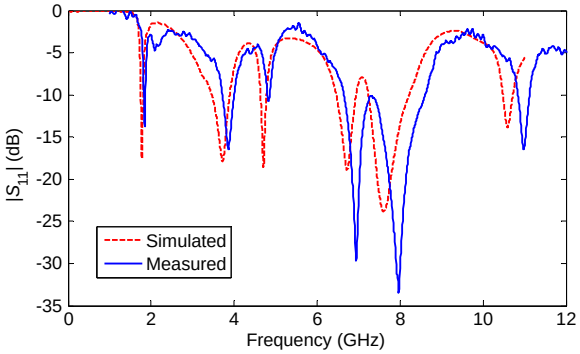

Figure 19. Measured and simulated $|S_{11}|$ responses of the proposed loaded dipole antenna of Figure 11 while the small rectangular patches are removed from the parasitic element.

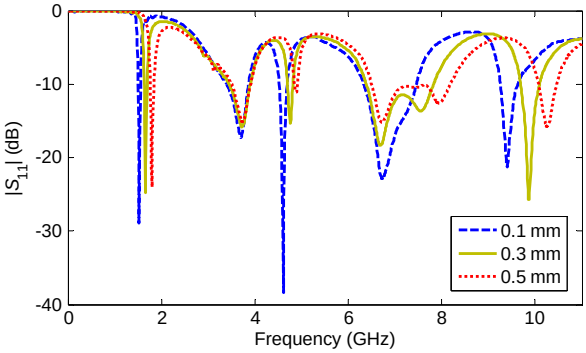

Figure 20. Simulated $|S_{11}|$ responses of the proposed loaded dipole antenna of Figure 11 for different widths of the printed thin strips of the parasitic element on the backside of the substrate.

of Figure 11 with removed small rectangular patches from the parasitic element, is fabricated. The reflection coefficient of the fabricated antenna of Figure 18 is measured and shown in Figure 19. There is a good agreement between the measured and simulated results.

Figure 20 shows the simulated reflection coefficients for a parametric study of the printed thin strips width on the backside of the substrate of loaded dipole antenna of Figure 11, which join the small rectangular patches together, while the other geometrical parameters are fixed. It can be observed that the width of the thin strips have an effective influence on the $|S_{11}|$ response of the proposed loaded dipole antenna of Figure 11. It should be noted that as the width is increased from 0.1 mm to 0.5 mm, the value of the lowest resonant frequency increases and therefore, the proposed loaded dipole antenna

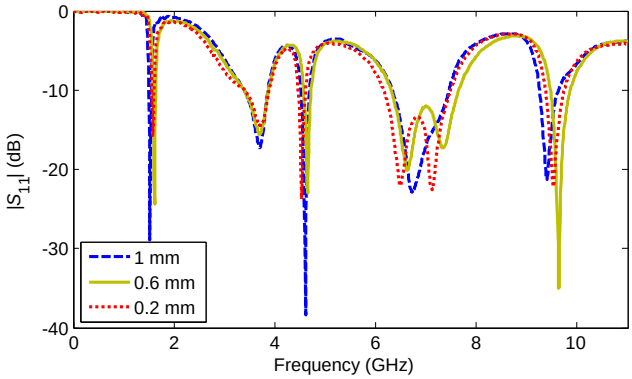

Figure 21. Simulated $|S_{11}|$ responses of the proposed loaded dipole antenna of Figure 11 for different widths of the capacitive gaps.

offers a lower degree of miniaturization. Furthermore, by increasing the width of thin strips, center frequencies of other resonance bands also increase.

The amount of series capacitances are related to the width of etched gaps on the dipole arms. The width of gaps are decreased from 1 mm to 0.2 mm in order to reveal the effect of series capacitive loadings on the resonant behavior of the proposed loaded dipole antenna of Figure 11, while the other geometrical parameters are fixed. Accordingly, the simulated reflection coefficients for different widths of the etched gaps, are plotted in Figure 21. It can be observed that with increasing the width of etched gaps from 0.2 mm to 1 mm, two resonance bands, between 6 GHz and 8 GHz, merge and create a single resonance band. In addition, we can infer that by altering the width of capacitive gaps, center frequencies of other resonance bands can be changed accurately. Based on the obtained results of demonstrated parametric studies, it is possible to control the resonance frequencies of the proposed loaded dipole antenna by altering its geometrical parameters.

4. CONCLUSION

We have demonstrated the designing procedure of a novel low-profile multiband fractal-inspired dipole antenna loaded with series capacitances and a parasitic element. The measured and simulated results reveal that when the designed host dipole antenna is loaded with series capacitances and a parasitic element, it offers more resonant frequency bands with high degree of miniaturization. The designed series capacitive loadings and parasitic element are able to improve the impedance matching of proposed dipole antenna. In addition, it is illustrated that by altering the various geometrical parameters of proposed antenna's elements, accurate control of the antenna's frequency bands can be obtained. Its compact size, planar structure, multiband and high-efficiency performance make it amenable for novel wireless applications.

REFERENCES

1. Quan, X. L., R. L. Li, Y. H. Cui, and M. M. Tentzeris, "Analysis and design of a compact dual-band directional antenna," *IEEE Antennas Wireless Propag. Lett.*, Vol. 11, 547–550, May 2012.
2. Salonen, P., M. Keskilammi, and M. Kivikoski, "Single-feed dual-band planar inverted-F antenna with U-shaped slot," *IEEE Antennas Wireless Propag. Lett.*, Vol. 48, No. 8, 1262–1264, Aug. 2000.
3. Guo, Y. X., K. M. Luk, and K. F. Lee, "Dual-band slot-loaded short circuited patch antenna," *Electron. Lett.*, Vol. 36, No. 4, 289–290, Feb. 2000.
4. Wong, K. L., L. C. Chou, and C. M. Su, "Dual-band-plate antenna with a shorted parasitic element for laptop applications," *IEEE Trans. Antennas Propag.*, Vol. 53, No. 1, 539–544, Jan. 2005.
5. Suh, Y. H. and K. Chang, "Low cost microstrip-fed dual frequency printed dipole antenna for wireless communications," *Electron. Lett.*, Vol. 36, 1177–1179, Jul 2000.

6. Kuo, Y. L. and K. L. Wong, "Printed double-T monopole antenna for 2.4/5.2 GHz dual-band WLAN operations," *IEEE Trans. Antennas Propag.*, Vol. 51, No. 9, 2187–2192, Sep. 2003.
7. Chou, L. C. and K. L. Wong, "Uni-planar dual-band monopole antenna for 2.4/5 GHz WLAN operation in the laptop computer," *IEEE Trans. Antennas Propag.*, Vol. 55, No. 12, 3739–3741, Dec. 2007.
8. Yang, H. Y. D. and Y. Y. Zhang, "A wideband miniaturized dipole antenna on a printed circuit board," *Progress In Electromagnetics Research C*, Vol. 10, 175–185, 2009.
9. Ku, C.-H. and H.-W. Liu, "Compact planar triple-band folded dipole antenna for WLAN/WiMAX applications," *Progress In Electromagnetics Research C*, Vol. 28, 1–13, 2012.
10. Li, X., L. Yang, S.-X. Gong, Y.-J. Yang, and J.-F. Liu, "A compact folded printed dipole antenna for UHF RFID reader," *Progress In Electromagnetics Research Letters*, Vol. 6, 47–54, 2009.
11. Abu, M. and M. K. A. Rahim, "Triple-band printed dipole tag antenna for RFID," *Progress In Electromagnetics Research C*, Vol. 9, 145–153, 2009.
12. Guo, Y. Y., X. M. Zhang, G. L. Ning, D. Zhao, X. W. Dai, and Q. Wu, "Miniaturized modified dipoles antenna for WLAN applications," *Progress In Electromagnetics Research Letters*, Vol. 24, 139–147, 2011.
13. Li, X., L. Yang, S.-X. Gong, and Y.-J. Yang, "Dual-band and wideband design of a printed dipole antenna integrated with dual-band balun," *Progress In Electromagnetics Research Letters*, Vol. 6, 165–174, 2009.
14. Zhang, R., G. Fu, Z.-Y. Zhang, and Q.-X. Wang, "A wideband planar dipole antenna with parasitic patches," *Progress In Electromagnetics Research Letters*, Vol. 20, 137–145, 2011.
15. Floc'h, J. M. and H. Rmili, "Design of multiband printed dipole antennas using parasitic elements," *Microw. Opt. Technol. Lett.*, Vol. 48, No. 8, 1639–1645, Aug. 2006.
16. Chang, K., H. Kim, and Y. J. Yoon, "A triple-band printed dipole antenna using parasitic elements," *Microw. Opt. Technol. Lett.*, Vol. 47, No. 3, 221–223, Nov. 2005.
17. Borja, A. L., "Dipole antenna with left-handed loading operating at a zero order mode," *Progress In Electromagnetics Research C*, Vol. 19, 85–92, 2011.
18. Caloz, C. and T. Itoh, *Electromagnetic Metamaterials, Transmission Line Theory and Microwave Applications*, John Wiley & Sons, Inc., Hoboken, NJ, USA, 2006.
19. Werner, D. H. and S. Ganguly, "An overview of fractal antenna engineering research," *Ant. Prop. Mag.*, Vol. 45, No. 1, 38–57, 2003.
20. Kimouche, H. and H. Zemmour, "A compact fractal dipole antenna for 915 MHz and 2.4 GHz RFID tag applications," *Progress In Electromagnetics Research Letters*, Vol. 26, 105–114, 2011.
21. Puente, C., J. Claret, F. Sagues, J. Romeu, M. Q. Lopez-Salvans, and R. Pous, "Multiband properties of a fractal tree antenna generated by electrochemical decomposition," *Electron. Lett.*, Vol. 32, No. 25, 2298–2299, 1996.
22. Werner, D. H., A. R. Bretones, and B. R. Long, "Radiation characteristics of thin-wire ternary fractal trees," *Electron. Lett.*, Vol. 35, No. 8, 609–610, 1996.
23. Petko, J. S. and D. H. Werner, "Miniature reconfigurable three-dimensional fractal tree antennas," *IEEE Trans. Antennas Propag.*, Vol. 52, No. 8, 1945–1956, Aug. 2004.
24. Li, D. and J.-F. Mao, "A Koch-like sided fractal bow-tie dipole antenna," *IEEE Trans. Antennas Propag.*, Vol. 60, No. 5, 2242–2251, May 2012.